Mono-photon at CEPC

Hao Liang
IHEP

2018

1 Introduction

CEPC is a proposed electron-positron collider, which circuference is 100 km. The center of mass energies of CEPC are 91.2GeV, 161GeV, and 240GeV, as Z boson, WW at threshold, and Higgs boson factories respectively. The operation plan is shown in Table 1.

Besides the main physical program, CEPC provide the opportunity of searching for new physics. Mono-photon process is one of processes to search new physics. The mono-photon process is important, because the photon could be used to tag the invisible particles in new physics. This note doesn't analyse the signal of mono-photon process in new physics, instead, it focus on the standard model (SM) background to serve the new physics study.

The mono-photon events in SM comes from invisible process plus a photon which is radiated from the incident particle (ISR) or the median particles (WW fusion). The invsible final states at are mainly from two process. The first is by a Z in s channel, the second is by a W in t channel. See Fig. 1 for the Feynman diagrams.

Operation mode	$\sqrt{s}$ [GeV]	L [ab^{-1}]
Z factory	91.2	10
WW threshold scan	161	2.6
H factory	240	5.6

Table 1: The operation plan of CEPC.

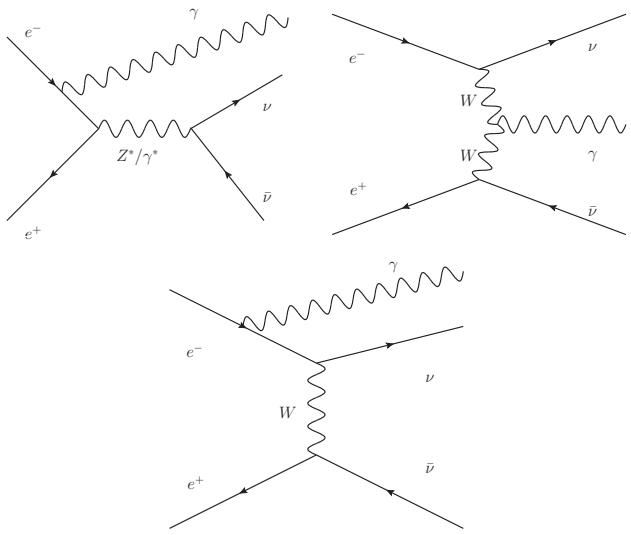

Figure 1: Feynman diagrams for mono-photon process.

2 The Method of Study

The differential events distributions at center of mass energies of 91.2GeV, 161GeV and 240GeV are shown in Fig. 2 respectively. We found the the cross sections of WW fusion in the lower energy are always negligible in the sensitve region. The 2-dimensional events distribution were attached in Appendix B.

The distribution of the photon in mono-photon process is fully described by the differential cross section $\frac{\mathrm{d}^2\sigma}{\mathrm{d}E_\gamma \mathrm{d}\cos(\theta)}$. We used Monte Carlo method to study the backgrounds. Whizard 1.9.5 was used to generate the events. The default ISR algorithm was used (so what algorithm?). In this algorithm, the beam is structured. The incident electron (positron) is thought as composite particle of electron (positron) and photons. The photon energy is sampled according to property distribution of energy fraction of energy, $x = E_\gamma/(\sqrt{s}/2)$. Two ISR photons will be generated, each is associated with a incident electron or positron. The leading photon (the photon with largest energy) is thought to be of interest.

See Fig. 3 for the energy distribution of the leading photon in process of s channel. The peak of return Z is wider than the one from the Z width and the there is a long tail at the left of the peak. This phenomenon can be explained by the convolution effect due to the sub-leading photon. The

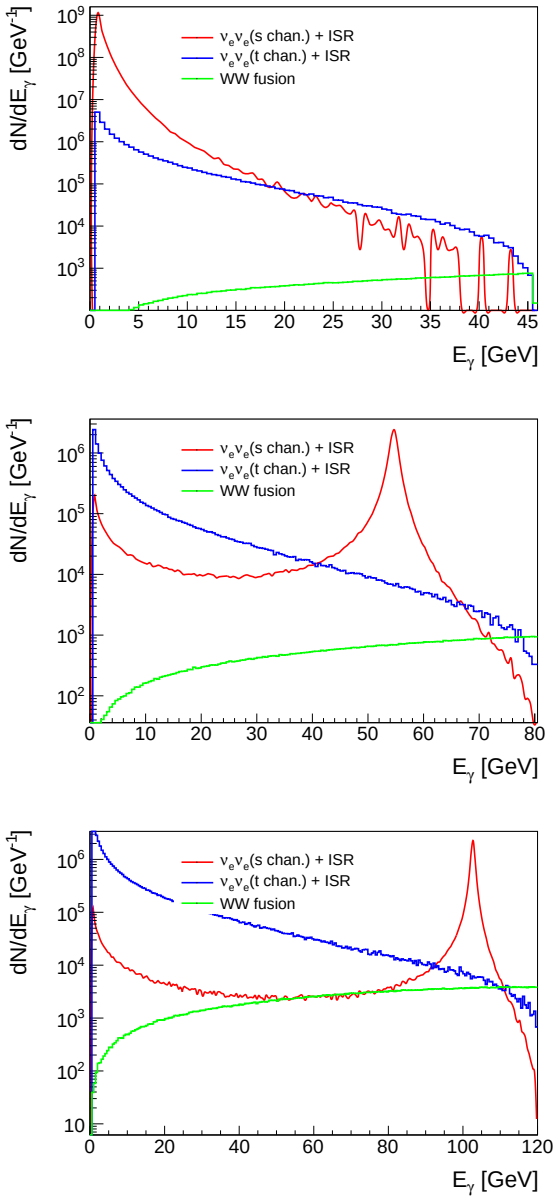

Figure 2: The differential cross section for the leading photon at center of mass energy of 91.2GeV, 161GeV, and 240GeV(from top to bottom respectively). The integral luminosities are corresponding to 10ab^{-1}, 2.6ab^{-1} and 5.6ab^{-1} respectively. A cut $|\cos(\theta_\gamma)| < 0.99$ is applied.

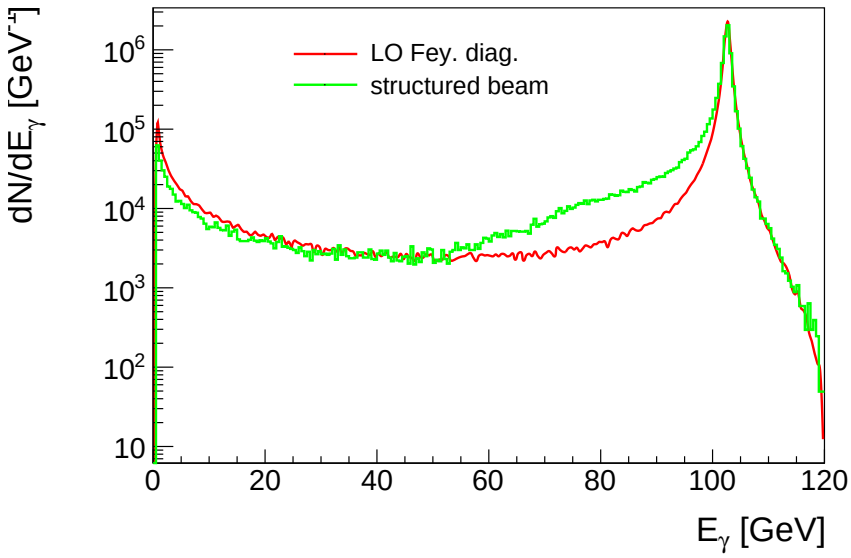

Figure 3: The Events distribution of the leading photon in process $Z(\nu_e\nu_e)$ + ISR at center of mass energy of 240GeV. A cut $|\cos(\theta_\gamma)| < 0.99$ is applied to let the comparison to be meaninglful.

result of direction calculation of leading order Feynman diagram in Fig. 1 is also shown in Fig. 3.

3 The Inclusive Mono-photon Distribution

The ISR photon as mono-photon includes $\nu_l\nu_l\gamma$ where $l = e, \mu, \tau$. The inclusive events distribution are shown in Fig. 4 for center of mass energies of 91.2GeV, 161GeV and 240GeV.

3.1 Smearing for finite energy resolution

The events distribution would be smeared with the detector energy resolution. See Fig. 5 for energy resolution of photon at CEPC for geometry of CEPCv4. The energy resolution has been parameterized in the form $\delta/E = \sqrt{a^2/E + b^2} = a/\sqrt{E} \oplus b$. A set of median values of a and b between the baseline and intrinsic, $a = 16\%$ and $b = 0.16\%$, were chosen for our study. The Smearing result for this set parameters is shown in Fig. 6.

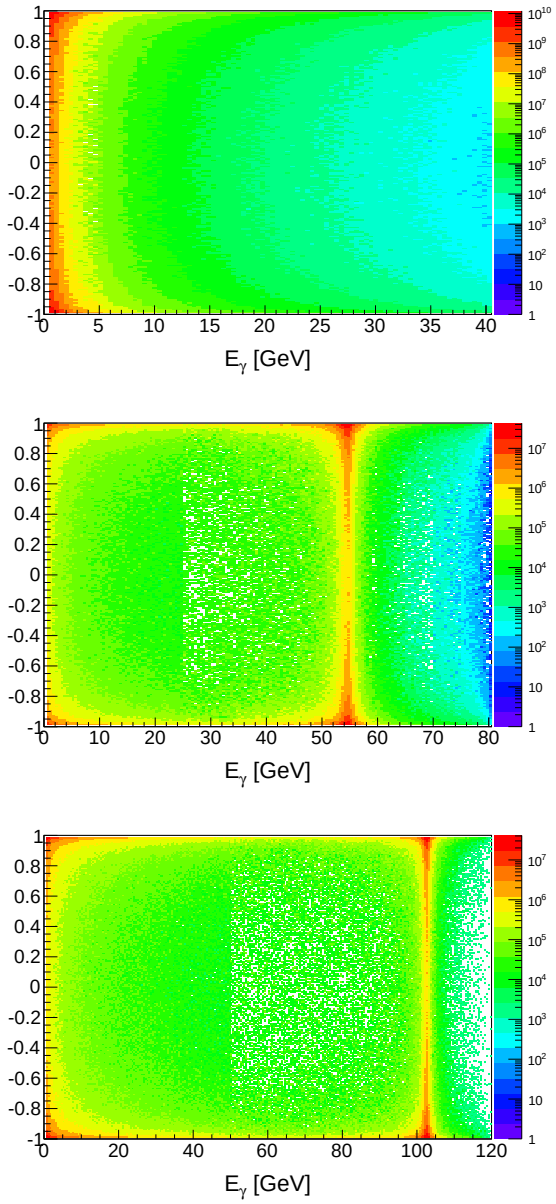

Figure 4: The number of events distribution of the leading photon at center of mass energy of 91.2GeV, 161GeV, and 240GeV(from top to bottom respectively). The integral luminosities are corresponding to 10ab^{-1}, 2.6^{-1} and 5.6 $^{-1}$ respectively. A cut $|\cos(\theta_\gamma)| < 0.99$ is applied.

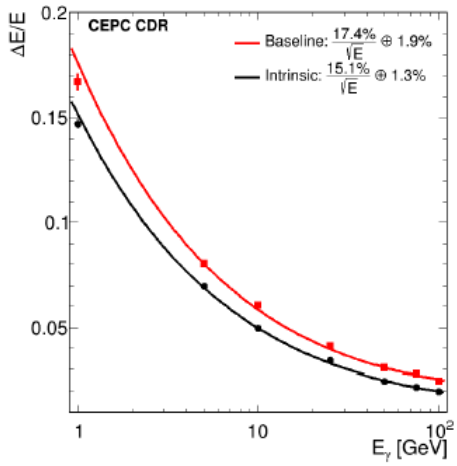

Figure 5: The energy resolution of photon at CEPC for geometry of CEPCv4.

The smearing were also preformed for various resolutions for studying the physics potential for the future detector design. See Appendix A for the smeared result with resolutions of $16\%/\sqrt{E} \oplus 1.6\%$, $3\%/\sqrt{E} \oplus 1.6\%$, $16\%/\sqrt{E} \oplus 0.3\%$, and $3\%/\sqrt{E} \oplus 0.3\%$.

3.2 Parameterization of the events distribution

For the ease of describe the photons distribution, the parameterization is needed. In the (what?) appximation,

$$\frac{\mathrm{d}\sigma}{\mathrm{d}E_\gamma \mathrm{d}\cos(\theta)} = \frac{\alpha_{\mathrm{EM}}}{\pi} \cdot \frac{1+(1-x)^2}{x} \cdot \frac{1}{\sin^2(\theta)} \cdot \sigma(ee^* \to \text{invisible}; \sqrt{s} - E_\gamma). \quad (1)$$

where $x = \frac{E_\gamma}{\sqrt{s}/2}$. Note that the angular and energy of photon is distributed inpdependently. Firstly, We assume this simplication true in the parameterization. So we need only to parameterize the mariginal distributions. The marginal distribution of energy and $\cos(\theta)$ from Monte Carlo are shown in the Fig. 7 and 8 respectively.

Secondly, for the angular differential distribution, we have test the factor $\sin(\theta)^{-2}$ is still precise enough for result of whizard. See Fig. 7.

Denote acceptance of detector as θ_c. The ISR cross-section is approximately proportional to $(\sin(\theta_\gamma))^{-2}$. So the total cross section in range

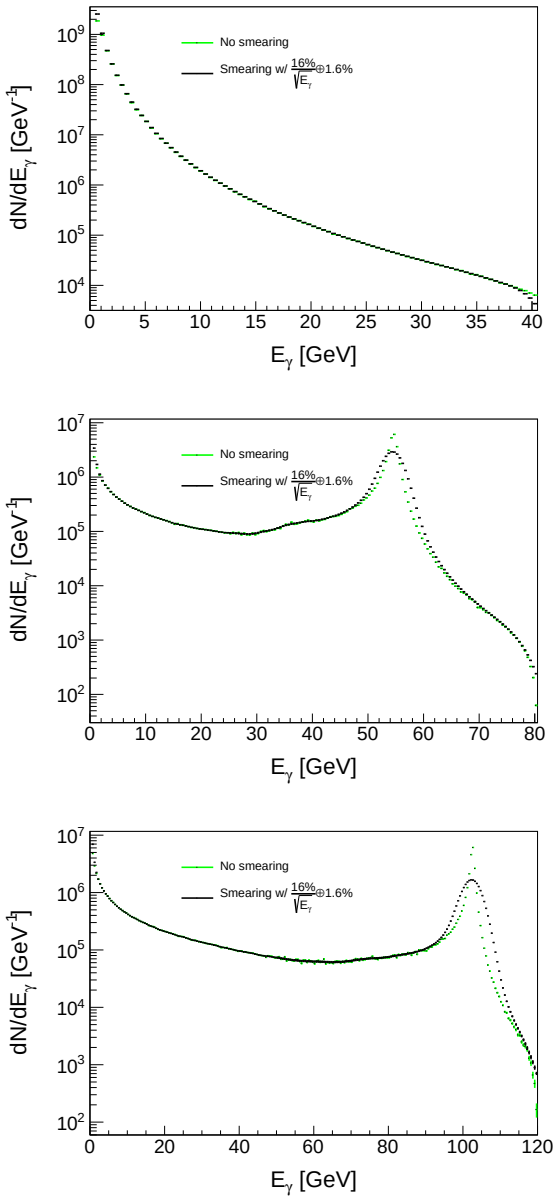

Figure 6: The number of events distribution, $\mathrm{d}N/\mathrm{d}E_\gamma$, of the leading photon at center of mass energy of 91.2GeV, 161GeV, and 240GeV (from top to bottom respectively). The integral luminosities are corresponding to $10\mathrm{ab}^{-1}$, $2.6\mathrm{ab}^{-1}$ and $5.6\mathrm{ab}^{-1}$ respectively. A cut $|\cos(\theta_\gamma)| < 0.99$ is applied.

$[-\cos(\theta), \cos(\theta)]$ is proportional to 2arctanh(cos(θ)). Although, the parameters c_i, and k is extract at $\theta_c = 0.99$, they are suitable for the other acceptance.

Note that for detector acceptance of cos(θ_c), the integral $\int 1/\sin(\theta)^2 \mathrm{d}\cos(\theta)$ results in 2arctanh(cos(θ_c)). By substituting the result into Eq. 1 and parameterizing $\sigma(ee^* \to \text{invisible}; \sqrt{s} - E_\gamma)$ as polynominal plus BreitWigner function, finally, we got the following form for fit

$$\frac{dN}{dE_\gamma} = \frac{\alpha_{\mathrm{EM}}}{\pi} \cdot \left(\frac{1+(1-x)^2}{x} + \frac{c_{-2}}{x^2}\right) \cdot 2\mathrm{arctanh}(\cos(\theta_c)) \cdot (N_1 + N_2) \qquad (2)$$

$$N_1 = c_0 + c_1 x + c_2 x^2 + c_3 x^3$$

$$N_2 = \frac{k(\Gamma_Z M_Z)^2}{(M^2_{\gamma\mathrm{recoil}} - M_Z^2)^2 + (\Gamma_Z M_Z)^2}$$

$$x = \frac{E_\gamma}{\sqrt{s}/2}$$

$$M_{\gamma\mathrm{recoil}} = \sqrt{(\sqrt{s} - E_\gamma)^2 - p_\gamma^2}$$

Note that additional term c_{-2}/x^2, were added for the smearing effect of detector. We have said the term c_{-2}/x^2 was added in Eq. 2 representing the detector smearing. The form of this term could be argumented by the Taylor expasion for the smearing. For an arbitrary function $f(E)$, the smeared function, $\bar{f}(E)$, by a normal function, Norm(E, δ), is given by

$$\bar{f}(E) = \int \mathrm{Norm}(E'-E,\delta) f(E') \mathrm{d}E' = \int \mathrm{Norm}(E'-E,\delta) \left(f(E) + \frac{1}{2}(E-E')^2 f''(E') \right) \mathrm{d}E'$$

$$\bar{f}(E) - f(E) \propto \delta^2 f''(E)$$

In our case, for $E \ll \sqrt{s}$, we have $f(E) \propto 1/E$, and $\bar{f}(E) - f(E) \propto \delta^2/E^3$. Substituting the $\delta^2 = a^2 E + b^2 E^2$ into the above formula, we finally got the $x^{-2} (\approx E^{-2})$ term in $\bar{f}(E) - f(E) \propto a^2/E^2 + b^2/E$.

See Table 3.2 for the parameters c_i and k.

4 Conclusion

In this note, we study the mono-photon process in SM. Firstly, we calculate the cross-section for t, s and WW fusion channels at leading oder. And we found the contribution from WW fusion is negligible. Secondly, we found

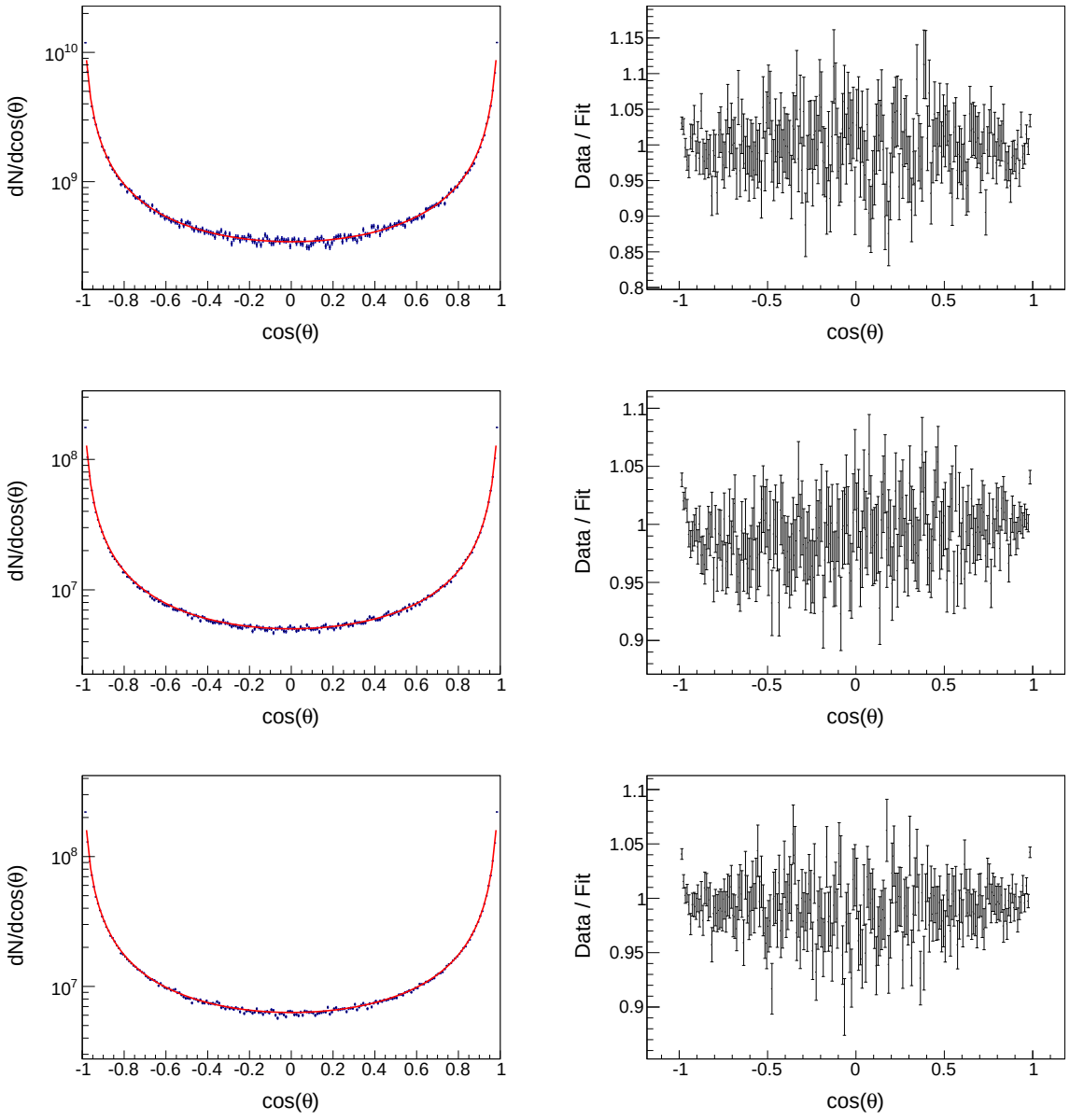

Figure 7: The number of events distribution, $\mathrm{d}N/\mathrm{d}\cos(\theta)$, of the leading photon at center of mass energy of 91.2GeV, 161GeV, and 240GeV (from top to bottom respectively). The integral luminosities are corresponding to 10ab^{-1}, 2.6^{-1} and 5.6 $^{-1}$ respectively. A cut $|\cos(\theta_\gamma)| < 0.99$ is applied. The data are fit in the form $C/(1-\cos^2(\theta))$.

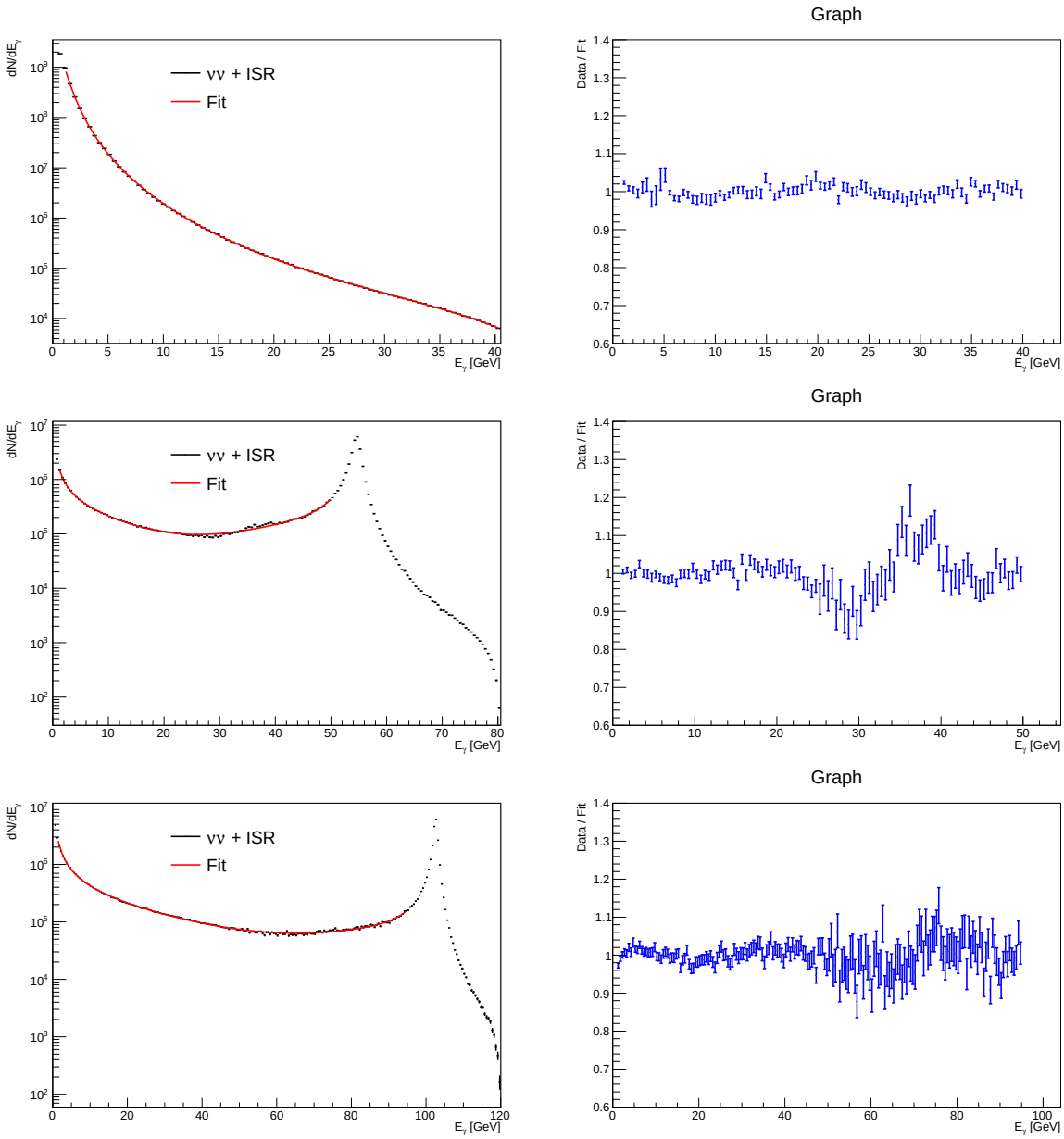

Figure 8: The number of events distribution, $\mathrm{d}N/\mathrm{d}E$, of the leading photon at center of mass energy of 91.2GeV, 161GeV, and 240GeV(from top to bottom respectively). The integral luminosities are corresponding to $10\mathrm{ab}^{-1}$, 2.6^{-1} and $5.6\ ^{-1}$ respectively. A cut $|\cos(\theta_\gamma)| < 0.99$ is applied.

Resolution	$\sqrt{s}$ [GeV]	Range[GeV]	c_{-2},c_0,c_1,c_2,c_3,k [GeV^{-1}]
Perfect detector	91.2	1 - 20	
	161	1 - 50	
	240	1 - 91	
$\sqrt{\frac{16\%}{\sqrt{E}} \oplus 1.6\%}$	91.2	1 - 20	
	161	1 - 50	
	240	1 - 91	
$\sqrt{\frac{3\%}{\sqrt{E}} \oplus 1.6\%}$	91.2	1 - 20	
	161	1 - 50	
	240	1 - 91	
$\sqrt{\frac{16\%}{\sqrt{E}} \oplus 0.3\%}$	91.2	1 - 20	
	161	1 - 50	
	240	1 - 91	
$\sqrt{\frac{3\%}{\sqrt{E}} \oplus 0.3\%}$	91.2	1 - 20	
	161	1 - 50	
	240	1 - 91	

Table 2: The fit parameters.

both ISR photons from two incident particles need to be considered in a process. Although, only the leading photon is of interest for measurement. The sub-leading photon has a non-negligible effect on the energy distribution of leading photon. Thirdy, the inclusive events distribution mono-photon are calculated. Then, the distribution were smeared with various energy resolution. Finally, the original and smeared distributions were parameterized for ease of use. The parameterization error is within 20% for smeared distributions and within 10% for original distribution.

A The Events Distribution with Smearing

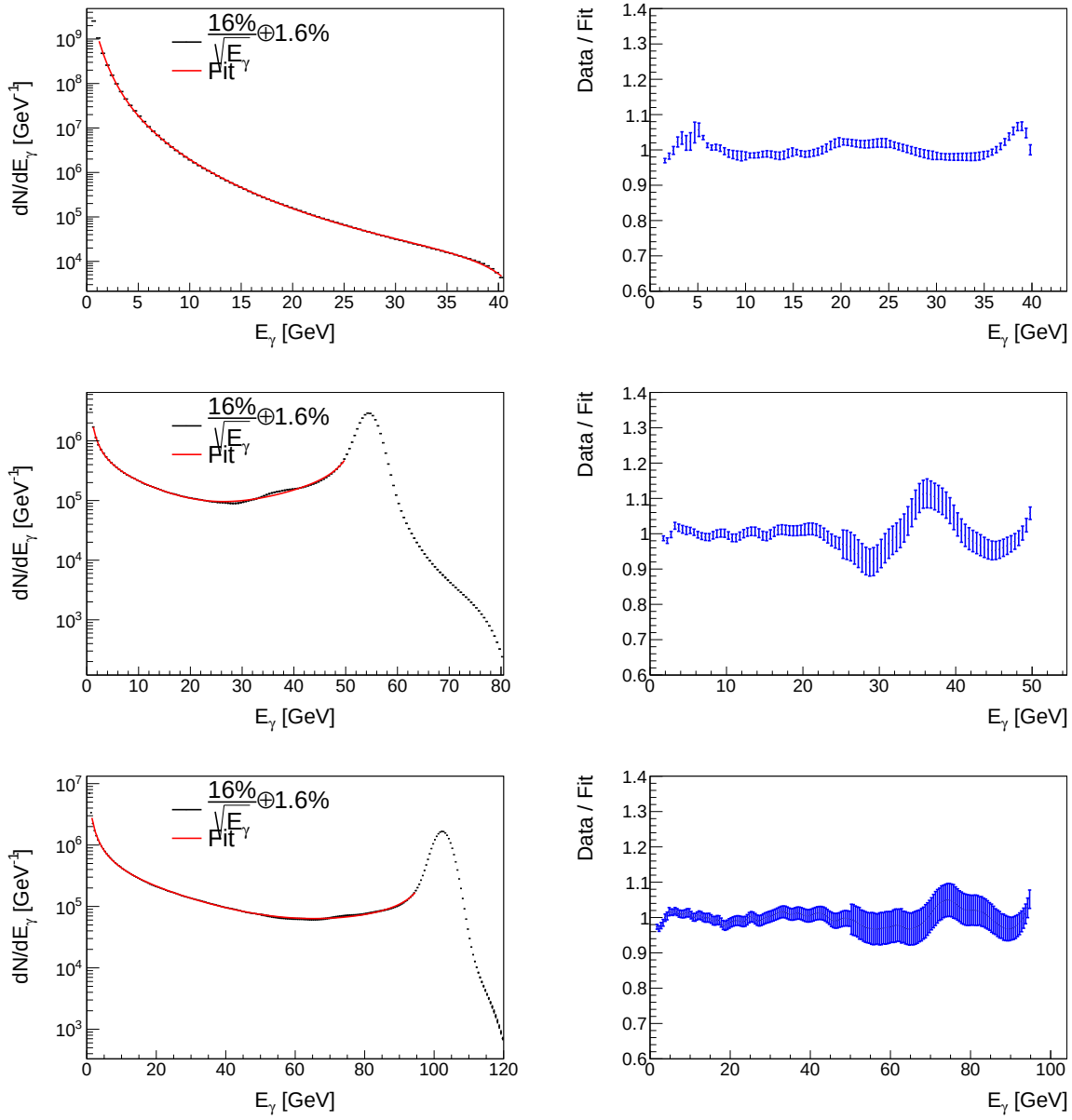

Figure 9: The number of events distribution, $\mathrm{d}N/\mathrm{d}E_\gamma$, of the leading photon at center of mass energy of 91.2GeV, 161GeV, and 240GeV (from top to bottom respectively). The integral luminosities are corresponding to $10\mathrm{ab}^{-1}$, $2.6\mathrm{ab}^{-1}$ and $5.6\mathrm{ab}^{-1}$ respectively. A cut $|\cos(\theta_\gamma)| < 0.99$ is applied.

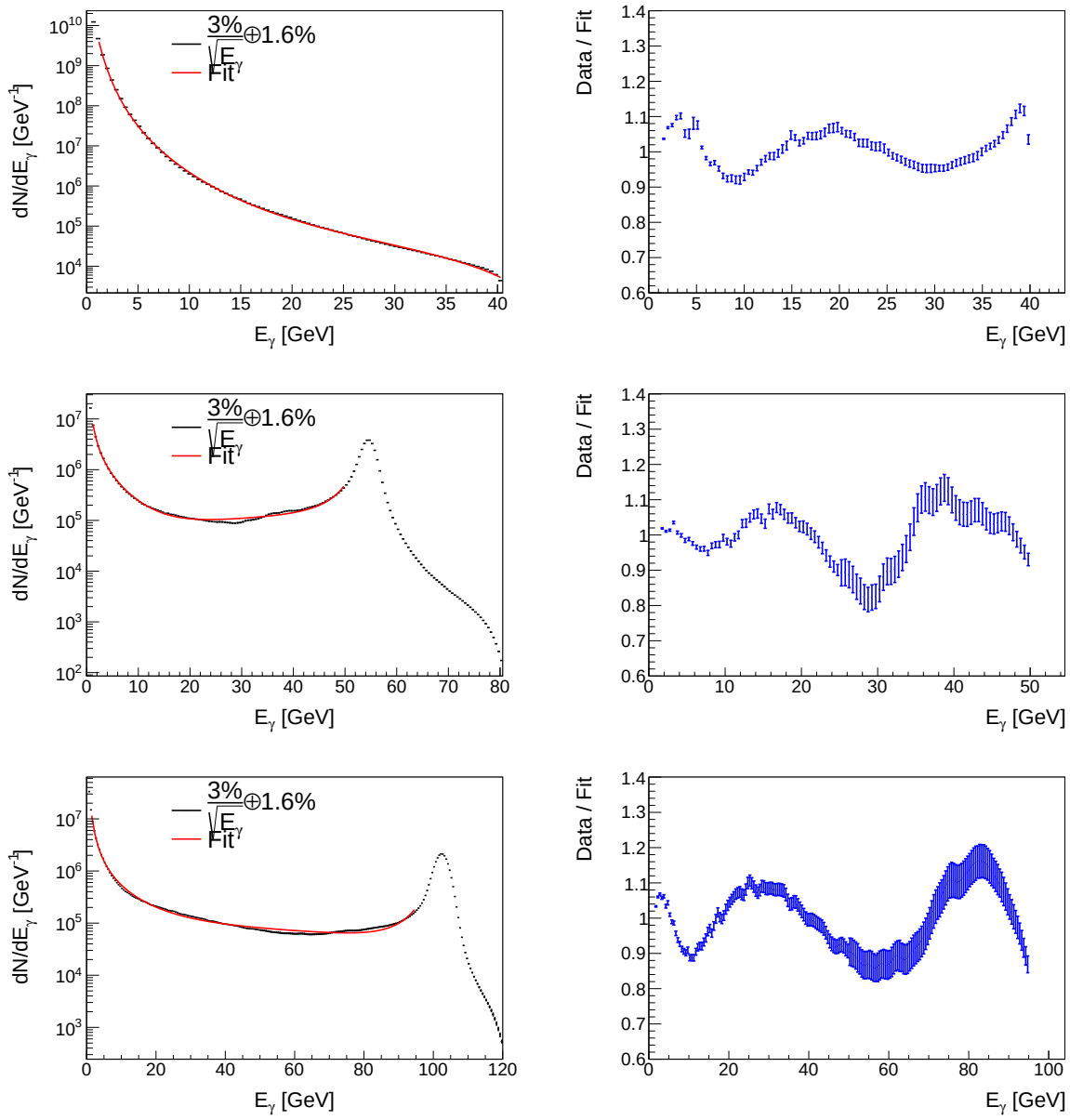

Figure 10: The number of events distribution, $\mathrm{d}N/\mathrm{d}E_\gamma$, of the leading photon at center of mass energy of 91.2GeV, 161GeV, and 240GeV (from top to bottom respectively). The integral luminosities are corresponding to $10\mathrm{ab}^{-1}$, $2.6\mathrm{ab}^{-1}$ and $5.6\mathrm{ab}^{-1}$ respectively. A cut $|\cos(\theta_\gamma)| < 0.99$ is applied.

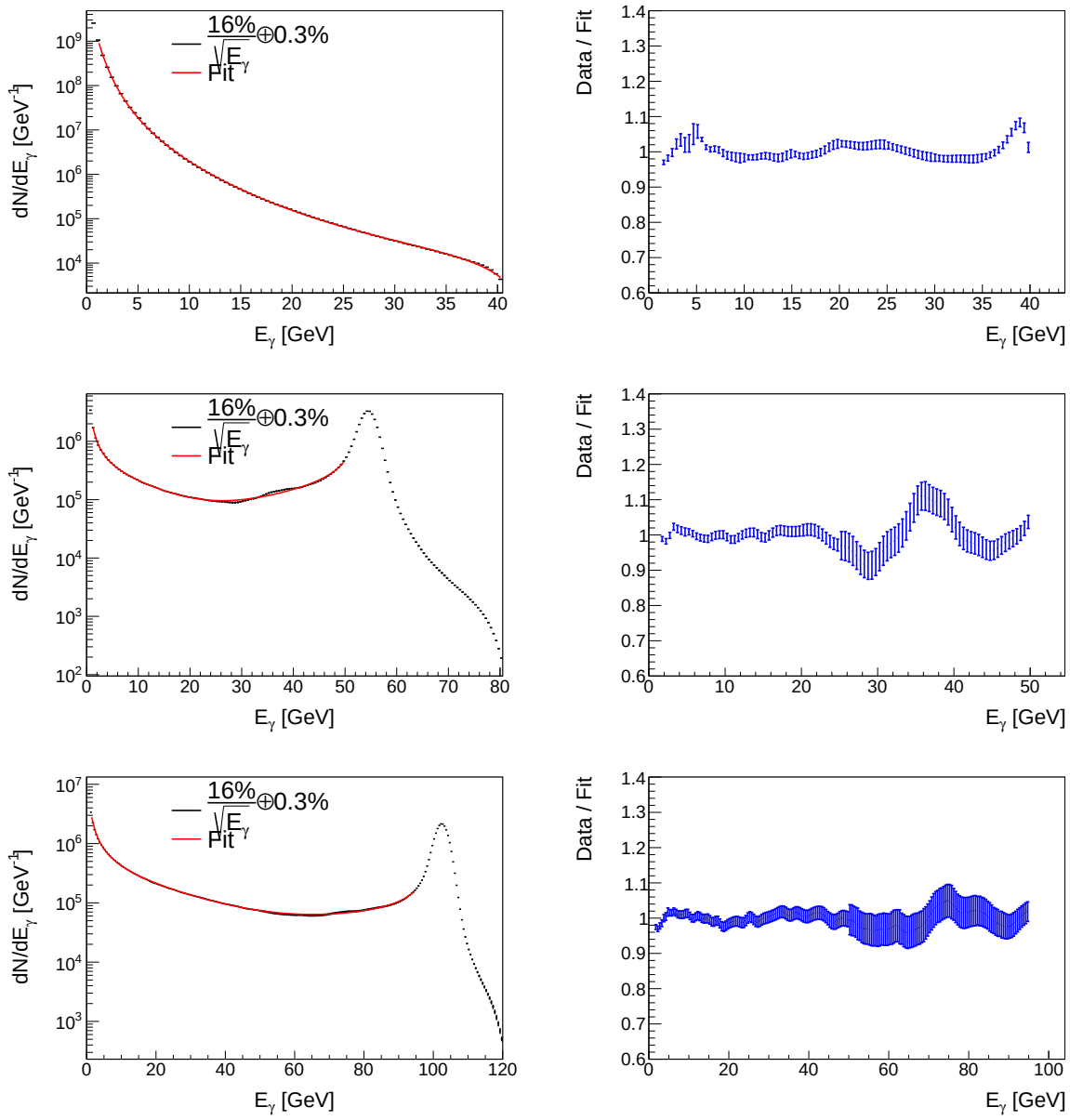

Figure 11: The number of events distribution, $\mathrm{d}N/\mathrm{d}E_\gamma$, of the leading photon at center of mass energy of 91.2GeV, 161GeV, and 240GeV (from top to bottom respectively). The integral luminosities are corresponding to $10\mathrm{ab}^{-1}$, $2.6\mathrm{ab}^{-1}$ and $5.6\mathrm{ab}^{-1}$ respectively. A cut $|\cos(\theta_\gamma)| < 0.99$ is applied.

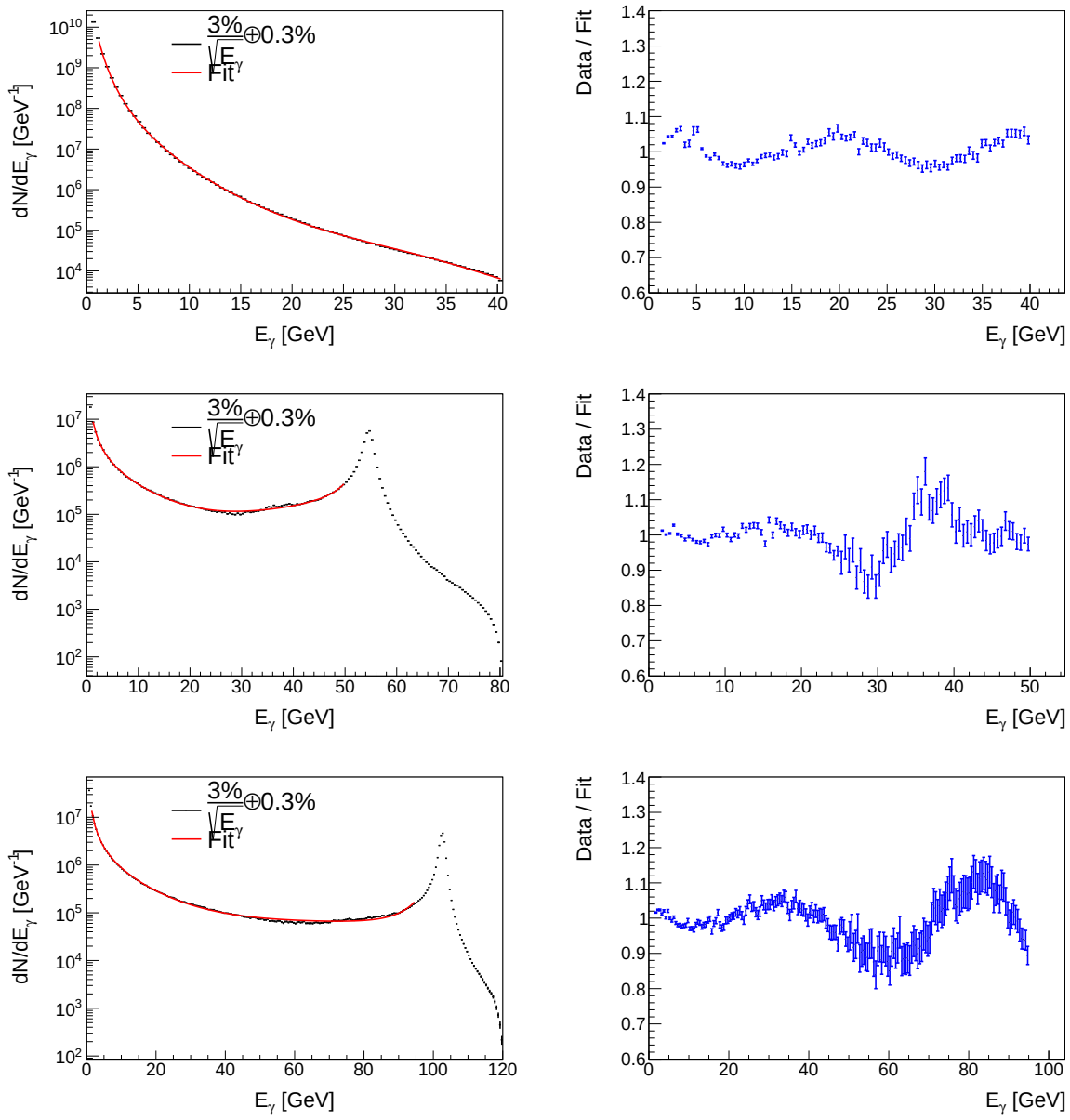

Figure 12: The number of events distribution, $\mathrm{d}N/\mathrm{d}E_\gamma$, of the leading photon at center of mass energy of 91.2GeV, 161GeV, and 240GeV (from top to bottom respectively). The integral luminosities are corresponding to $10\mathrm{ab}^{-1}$, $2.6\mathrm{ab}^{-1}$ and $5.6\mathrm{ab}^{-1}$ respectively. A cut $|\cos(\theta_\gamma)| < 0.99$ is applied.

B Events Distributions for Sub-channels

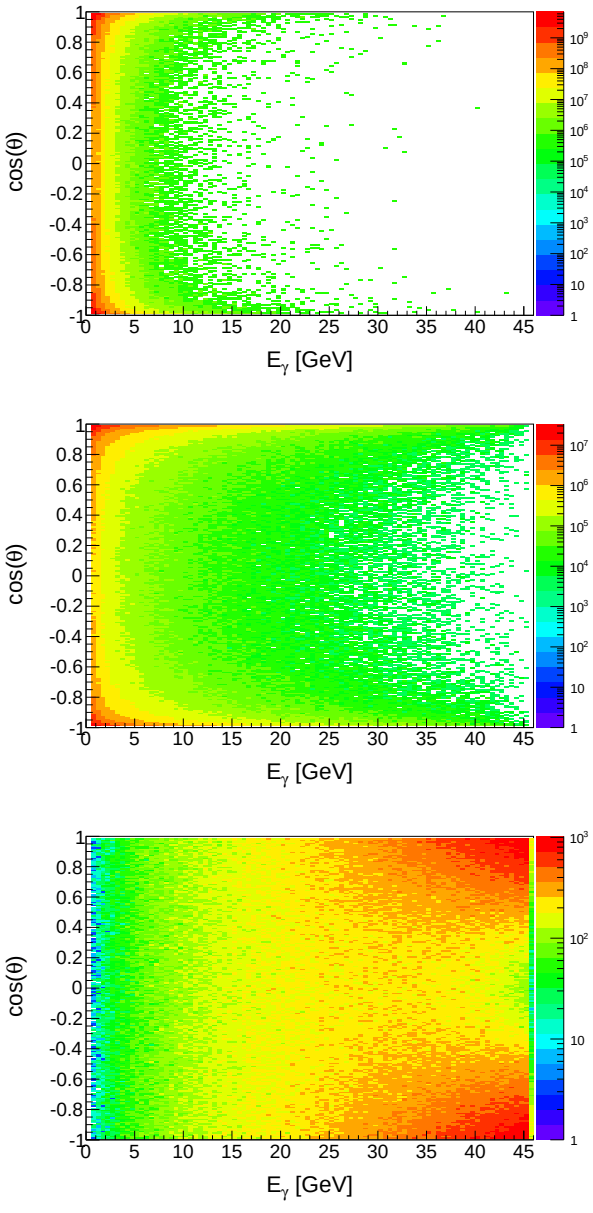

Figure 13: Events distribution for center of mass energy of 91.2GeV. From top to bottom, they are $\nu_e\nu_e$(s channel) + ISR, $\nu_e\nu_e$ (t channel) + ISR, and WW fusion. The integral luminosity is the same in Fig. 4.

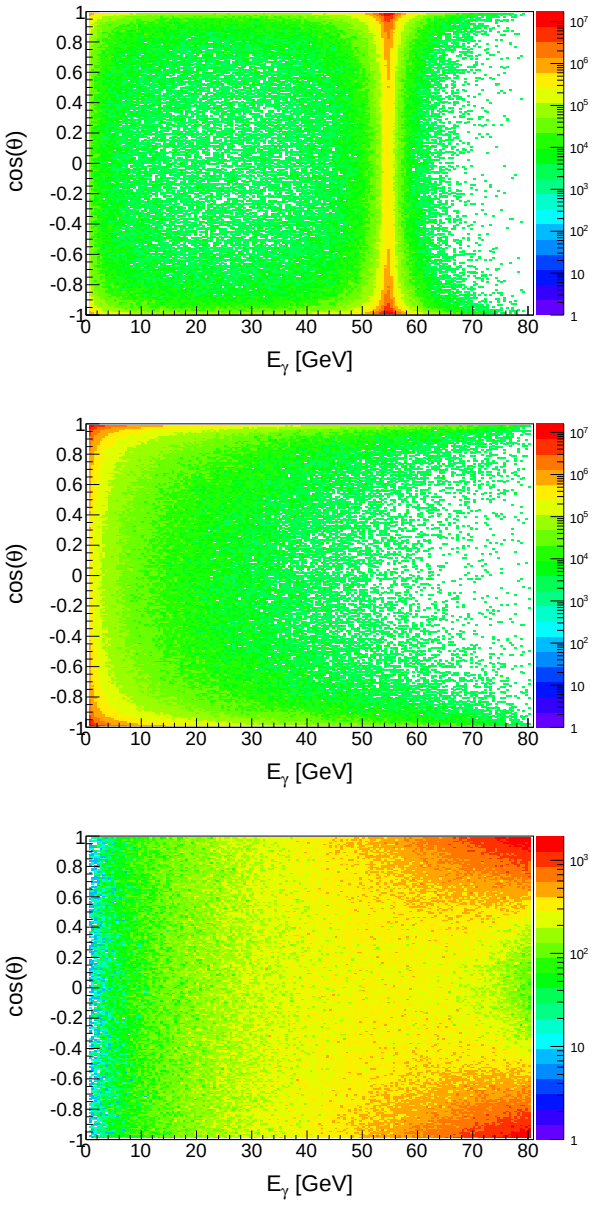

Figure 14: Same as Fig. B, but for center of mass energy of 161GeV.

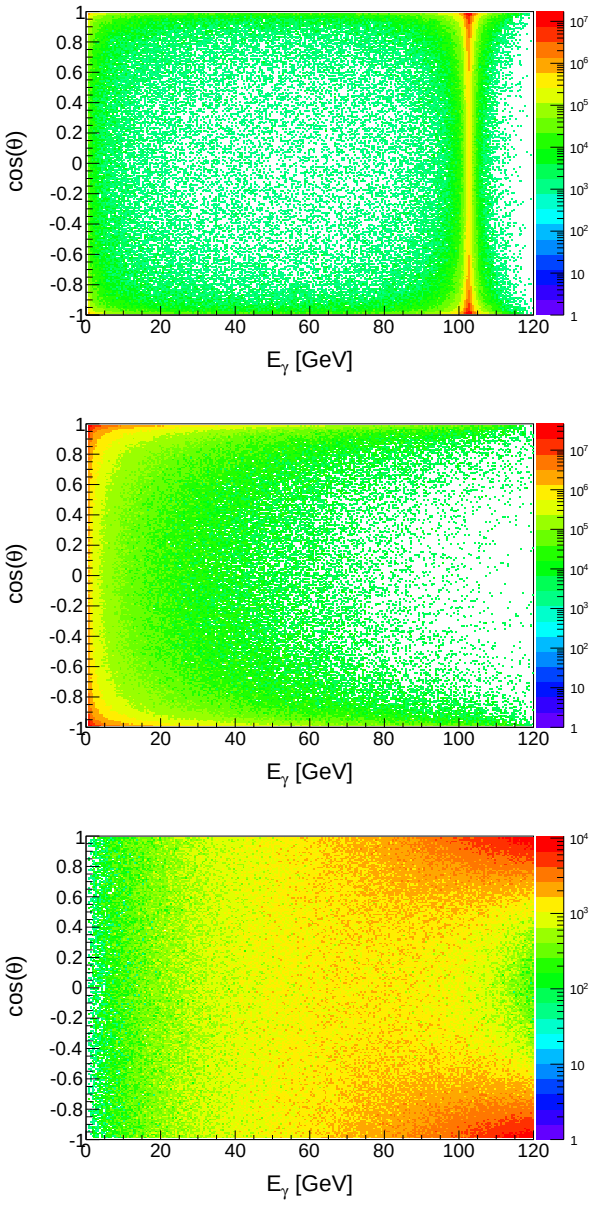

Figure 15: Same as Fig. B, but for center of mass energy of 240GeV.